International Journal of Nanomedicine

Dovepress
open access to scientific and medical research

Open Access Full Text Article

ORIGINAL RESEARCH

Gestational Diabetes Mellitus Impedes Fetal Lung Development Through Exosome-Dependent Crosstalk Between Trophoblasts and Lung Epithelial Cells

Pengzheng Chen[1], Mengqi Gu[1], Shuting Wan[1], Xiaotong Jiang[1], Fengyuan Zhang[2], Yuchen Li[2], Qian Zhou[2], Yuan Lu[2], Lei Li[1–3], Xietong Wang[1–4]

[1]Department of Obstetrics and Gynaecology, Shandong Provincial Hospital, Shandong University, Jinan, People's Republic of China; [2]Department of Obstetrics and Gynaecology, Shandong Provincial Hospital Affiliated to Shandong First Medical University, Jinan, People's Republic of China; [3]Laboratory of Medical Science and Technology Innovation Center (Institute of Translational Medicine), Shandong First Medical University (Shandong Academy of Medical Sciences), Jinan, People's Republic of China; [4]Key Laboratory of Birth Regulation and Control Technology of National Health Commission of China, Shandong Provincial Maternal and Child Health Care Hospital, Jinan, People's Republic of China

Correspondence: Lei Li; Xietong Wang, Department of Obstetrics and Gynaecology, Shandong Provincial Hospital, Shandong University, Jinan, People's Republic of China, Tel +8615168889200; +8615168888928, Email lilei@sdfmu.edu.cn; 198657000067@email.sdu.edu.cn

Background: Fetal lung underdevelopment (FLUD) is associated with neonatal and childhood severe respiratory diseases, among which gestational diabetes mellitus (GDM) play crucial roles as revealed by recent prevalence studies, yet mechanism underlying GDM-induced FLUD, especially the role of trophoblasts, is not all known.

Methods: From the perspective of trophoblast-derived exosomes, we established in vitro, ex vivo, in vivo and GDM trophoblast models. Utilizing placenta-derived exosomes (NUB-exos and GDMUB-exos) isolated from normal and GDM umbilical cord blood plasma and trophoblast-derived exosomes (NC-exos and HG-exos) isolated from HTR8/SVneo trophoblasts medium with/without high glucose treatment, we examined their effects on fetal lung development and biological functions.

Results: We found that, compared with the NUB-exos group, the exosome concentration increased in GDMUB-exos group, and the content of exosomes also changed evidenced by 61 dysregulated miRNAs. After applying these exosomes to A549 alveolar type II epithelial cells, the proliferation and biological functions were suppressed while the proportion of apoptotic cells was increased as compared to the control. In ex vivo studies, we found that GDMUB-exos showed significant suppression on the growth of the fetal lung explants, where the number of terminal buds and the area of explant surface decreased and shrank. Besides, the expression of Fgf10, Vegfa, Flt-1, Kdr and surfactant proteins A, B, C, and D was downregulated in GDMUB-exos group, whilst Sox9 was upregulated. For in vivo studies, we found significant suppression of fetal lung development in GDMUB-exos group. Importantly, we found consistent alterations when we used NC-exos and HG-exos, suggesting a dominant role of trophoblasts in placenta-derived exosome-induced FLUD.

Conclusion: In conclusion, GDM can adversely affect trophoblasts and alter exosome contents, causing crosstalk disorder between trophoblasts and fetal lung epithelial cells and finally leading to FLUD. Findings of this study will shine insight into the theoretical explanation for the pathogenesis of FLUD.

Keywords: gestational diabetes mellitus, fetal lung underdevelopment, trophoblast, placenta-derived exosome, trophoblast-derived exosomes

Introduction

Gestational diabetes mellitus (GDM) is defined as glucose intolerance with onset or first recognition during pregnancy,[1] and it imposes short- and long-term risks on mothers and developing fetuses. Epidemiologically, GDM has been recognized as one of the most common obstetric complications at 6.1% to 15% occurrence worldwide,[2] potentially

Received: 12 November 2022
Accepted: 2 February 2023
Published: 8 February 2023

associated with increased risks of various adverse pregnancy outcomes, including congenital anomalies, cardiac malformations, neural tube defects, macrosomia, shoulder dystocia, and perinatal morbidity and mortality.[3–6] Over recent years, GDM is more and more proved to be an unneglectable etiology of fetal lung underdevelopment and delayed lung maturation that results in after-birth respiratory distress[7–9] and neonatal persistent pulmonary hypertension[10] at birth and even progression to chronic lung disease in the future. Inadequate production of surfactant proteins, which can decrease the alveolar surface tension to increase lung compliance and prevent alveolar collapse at the end of expiration, is considered to be the major cause of fetal lung underdevelopment and delayed lung maturations in GDM.[11] Antenatal corticosteroid is considered to be one of the most effective treatments. However, recent studies revealed the potential adverse effects of antenatal corticosteroid on fetal neurodevelopment and even contributed to mental and behavioral disorders in children.[12,13] Therefore, there is an urgent need to explore the exact aetiology and pathogenesis of GDM-induced FLUD.

Placenta can functionally integrate maternal exposures and provides hormones, cytokines, oxygen, and nutrients to maintain fetal development.[2] Besides, as a natural interface between mother and fetus, placenta is vulnerable to GDM-induced intrauterine environmental changes. For example, placenta can alter the expression of various molecules such as interleukins, leptin, and TNF-α receptors in response to maternal hyperglycemia and participates in inflammation reaction, innate defense, endocrine response, and oxidative stress.[14,15] Given the great structural and functional similarities between placenta and fetal lung, the fetal lung underdevelopment may be potentially associated with dysfunctions of placenta.[16] More convincingly, the perturbation of "placenta-fetal lung" connection has been determined to play crucial roles in fetal lung underdevelopment due to placental disorders during pregnancy,[17] thereby the placenta adaptation to hyperglycemic environment deserves more attention regarding fetal lung underdevelopment.

Exosomes derived from placenta have been reported to play vital roles in maternal–fetal interface communication.[18] Exosomes are nano-sized vesicles ranging from 30 to 200 nm in diameter, and they are released into surrounding body fluids upon fusion of multivesicular bodies and the plasma membrane.[19] Evidenced by previous studies, the concentration of placenta-derived exosomes significantly increased in GDM-complicated pregnancies at all stages of gestational pregnancies.[20] And hyperglycemia (glucose, 25 mM) can enhance exosomes release from trophoblasts.[21] Also, placenta-derived exosomes are found to change the function of endothelial cells[22] or skeletal muscle insulin sensitivity[23] in maternal circulation system. Functionally, exosomes can encapsulate a variety of biological substances such as proteins, mRNAs, and microRNAs (miRNAs), which enable them to deliver information of parent cells to recipient cells in various diseases.[24,25] Nevertheless, little is known about the alteration of placenta-derived exosomes such as concentration, content, and biological functions in GDM-associated fetal lung underdevelopment.

Herein, we isolated and characterized placenta-derived exosomes from umbilical cord blood plasma of healthy control and GDM subjects (denoted as NUB-exos and GDMUB-exos) and profiled exosomal miRNAs at genome-wide level. By establishing in vitro, ex vivo and in vivo models, we examined the effects of exosomes on fetal lung development. In parallel, we show the biological effects of HTR8/SVneo trophoblasts-derived exosomes on fetal lung development. These findings would provide new insights to clarify the involvement of placenta- and trophoblast-derived exosomes on fetal lung underdevelopment in GDM.

Materials and Methods

Human Umbilical Cord Blood Plasma Samples

All GDM and healthy gestational age-matched umbilical cord blood samples were collected from patients who delivered at Shandong Provincial Hospital affiliated to Shandong University. A 75 g OGTT was performed for GDM diagnosis: a fasting plasma glucose level ≥5.1 mmol/L and/or a glucose level ≥10.0 mmol/L at 1 h and/or ≥8.5 mmol/L at 2 h after a 75 g oral glucose load, and followed the cut-off by guidelines from the National Institute of Clinical Excellence.[26] Women with multiple pregnancies, prepregnancy diabetes, cardiovascular disease, or preeclampsia were excluded. The control group was defined as gestational age-matched women without abnormal OGTT results and the clinical characteristics are shown in Table S1. Blood samples from the GDM patients and controls were collected in 4-mL vacutainer tubes with K2EDTA anticoagulant (BD, USA), gently inverted and then shipped at 4°C within 1 hour after collection.

For harvesting plasma, blood samples were centrifuged at 2000 × g for 15 min at 4°C, and 1 mL fractions of the supernatants were transferred into fresh 1.5 mL tubes and stored at −80°C before use. Written informed consent was obtained before patients and healthy controls were recruited for the study, and this study was performed under the Declaration of Helsinki and approved by the Committee for Ethical Review of Research involving Human Subjects of Shandong Provincial Hospital.

Cell Culture

Human alveolar epithelial type II A549 cells were purchased from Bluefbio Biology Technology Development Co., Ltd (Shanghai, China). The first-trimester human extravillous trophoblast cell line HTR-8/SVneo cells were purchased from the American Type Culture Collection (Manassas, VA). A549 cells were maintained in high-glucose Dulbecco's modified Eagle's medium (DMEM, Gibco) supplemented with 10% fetal bovine serum (Gibco) and 1% penicillin-streptomycin (Gibco). HTR8/SVneo cells were cultured in RPMI 1640 medium (Gibco) supplemented with 10% exosome-free fetal bovine serum (Gibco) and 1% penicillin-streptomycin (Gibco) with/without 25mM high glucose. All cells were maintained in a 5% CO2 incubator at 37°C.

Exosomes Isolation and Characterization

Placenta-derived exosomes from umbilical cord blood plasma were isolated by a series of centrifugation strategies combined with sucrose density gradient centrifugation as previously described with modifications.[27–29] Briefly, a total of 5 mL of plasma was mixed with equal volume of cold phosphate-buffered saline (PBS) and centrifuged at 300 × g for 10 min, 2000 × g for 30 min, and 12,000 × g for 45 min to separate cell debris and other macromolecules. The resultant supernatant fluid was passed through a 0.22-μm sterile filter (Steritop; Millipore) and then ultracentrifuged at 120,000×g for 120 min (Beckman Coulter). The pellets were resuspended in 0.25 M sucrose and loaded onto a linear sucrose gradient with layers of 1.03, 1.06, 1.09, 1.11, 1.14, and 1.18 g/mL sucrose followed by ultracentrifugation at 200,000 × g for 16 h using swing bucket centrifuge rotors (Beckman Coulter). Subfractions containing different densities were sequentially extracted from the top of the sample tube and an equal volume of sample from each fraction was analysed by SDS–PAGE with placenta-derived exosome marker proteins. Then, the suspension containing placenta-derived exosomes was resuspended in ice-cold PBS and ultracentrifuged at 120,000 × g for 70 min twice. HTR8/SVneo cell supernatants were centrifuged in accordance with that of plasma and ultimately ultracentrifuged at 120,000 × g for 70 min twice. The pellets were resuspended in 200 μL of PBS. All procedures were performed at 4°C. The concentrated exosomes were stored at –80°C or used for the subsequent experiments. The exosome morphology was measured by transmission electron microscopy (HT7700, Hitachi, Japan) in the laboratory of Shandong Second Provincial General Hospital. The particle concentrations and size distributions were measured by nanoparticle tracking analysis on a NanoSight NS300 (Malvern).

Western Blot

All proteins were extracted using RIPA-PMSF methods and quantified through BCA kit (Solarbio, Beijing, China). Briefly, 20 μg of loaded protein was separated with 7.5%, 10% or 12.5% SDS–PAGE (Epizyme, Shanghai, China), and then transferred onto PVDF membranes (Millipore, MA, USA). The membranes were blocked with 5% nonfat milk at room temperature for 1 h and incubated at 4°C overnight with the primary antibodies. The next day the membranes were incubated with the corresponding secondary antibody (Proteintech) for 2 h. Finally, the blots were visualized by Amersham Imager 600 system (GE, Boston, MA, USA). The relative quantitative values of the bands were measured by ImageJ software. Each assay was repeated three times.

Primary antibodies at 1:1000 dilution used for Western blotting were as follows: CD63 (ab134045; Abcam), TSG101 (ab125011; Abcam), PLAP (ab133602; Abcam), SPA (ab87674, Abcam; ab115791, Abcam), SPB (ab271345, Abcam; ab231551, Abcam), SPC (ABC99, Sigma-Aldrich; ab211326, Abcam), SPD (sc-25324, Santa Cruz Biotechnology; ab220422, Abcam), Sox9 (ab185966, Abcam), Bim (C34C5, CST), Bax (#2772, CST), Bcl2 (D17C4, CST), Cleaved Caspase-3 (1:500, 5A1E, CST) and tubulin (#2146, CST) as a control.

Animals Maintenance and Intervention

Ten-week-old C57BL/6J mice were purchased from Jinan Peng Yue Laboratory Animal Breeding Co., Ltd., and were bred in the animal care facility at the animal laboratory of Shandong Provincial Hospital. All mice were housed in a temperature-controlled room with a 12:12-hr light/dark cycle. The mice were mated at night, and on the second day, we checked the appearance of a vaginal plug and counted 0.5 days post-coitum (E0.5) if positive. All animal experiments were approved by the Ethics Committee of Shandong Provincial Hospital and conducted in strict conformity with China's Guidelines for the Ethical Review of Laboratory Animal Welfare (GBT 35892–2018).

The fetal lung explants were isolated from E11.5 embryos as published with a stereomicroscope,[30] transferred onto a 24-mm clear polyester membrane Transwell supports with a 0.4-μm pore size (Corning) and cultured at the air-liquid interface in DMEM/F12 medium (Gibco) and 10% exosome-free fetal bovine serum with a humidified atmosphere of 95% air/5% CO_2 at 37°C. After 12 h culture, the explants were treated with medium only, medium + NUB-exos (200 μg/mL), medium + GDMUB-exos (200 μg/mL), medium + NC-exos (200 μg/mL) or medium + HG-exos (200 μg/mL) for 72 h. The number of terminal buds and lung surfaces were monitored every 24 h by taking photos on a light microscope (Olympus), and the differences between 0 h and 72 h are expressed as the D3/D0. After 72 h culture, the lung explants were harvested and immediately frozen at −80°C for protein and RNA extractions or were fixed in 4% paraformaldehyde and embedded in paraffin.

The intra-amniotic injections were conducted at E14.5. Briefly, pregnant mice were anesthetized by intraperitoneal administration of 350 μL of tribromoethanol and then were positioned on a heating pad and stabilized with adhesive tape. After disinfection with iodophor, we used sterile scissors to dissect the abdominal cavity and recorded the number of fetuses. With a Hamilton syringe, NUB-exos, GDMUB-exos, NC-exos or HG-exos at concentrations of 500 μg per 50 μL of 1x sterile PBS were injected intra-amniotically into the gestational sac. In the blank group, the amniotic cavities were only penetrated, and the control group was injected only with 50 μL of 1x sterile PBS. The total time of the procedure (from initial anesthesia) was approximately 20–25 min, and there was no incidence of maternal demise. On E18.5, the mice were sacrificed, and the fetuses were harvested by cesarean section. Due to the influence of fetal sex on fetal lung development, the ratio of male to female fetal mice used in these experiments is 1:1. Then the fetal weight and crown-rump length (CRL) were recorded. The lungs were dissected and immediately frozen at −80°C for protein and RNA extraction or fixed in 4% paraformaldehyde and embedded in paraffin.

Exosome Labeling and Internalization

To determine whether exosomes can be effectively absorbed, purified exosomes were labeled with PKH67 according to the manufacturer's instructions (MIDI67, Midi kit, Sigma-Aldrich). Excess dye was removed by centrifuging the exosomes at 100,000 × g for 60 min. The labeled exosomes were resuspended in PBS.

In intro assays, PKH67-labeled exosomes were added to 60% confluent A549 cells for 24h, and then the cytoskeleton and nucleus were labelled with phalloidin-iFluor 594 (ab176757, Abcam) and DAPI (Solarbio) respectively. Finally, the samples were imaged using ImageXpress Micro Confocal with MetaXpress software.

In ex vivo assays, PKH67-labeled exosomes were added to the lung explants and cultured for 72 hours. The lung explants were washed three times with 1 x PBS, then transferred to slides, and sealed with anti-fluorescence quenching mounting media. Finally, the lung explants were imaged using an inverted fluorescence microscope (Nikon, Tokyo, Japan) (4 x objective).

In in vivo assays, we intra-amniotically injected E14.5 mice with PKH67-labeled exosomes. After 24 h, the fetal lung was collected and digested with DNase and collagenase Type IV (Solarbio) for 45 min at 37°C. Digested tissues were then incubated in red blood cell lysis buffer (Solarbio) followed by straining with a 40 μm cell strainer. Cell flow-through was then pelleted and washed with 1x PBS twice, then resuspended with DMEM/F12 containing 10% FBS to prepare a single cell suspension. Finally, single cells from different groups injections were seeded in 96-well plates and incubated in a 5% CO2 incubator at 37°C for 24 h. The procedures were under dark conditions. The next day, we labelled the cytoskeleton and nucleus with phalloidin-iFluor594 (ab176757, Abcam) and DAPI (Solarbio) respectively, and imaged the cells using ImageXpress Micro Confocal with MetaXpress software.

CCK8 Assay

Cell Counting Kit-8 reagent, based on WST-8, is widely used in cell proliferation assays. In the presence of electron coupling reagents, WST-8 can be reduced by some dehydrogenases in mitochondria to produce orange-yellow formazan. The shade of color (the amount of formazan produced) is linearly related to the number of cells. A549 cells were seeded in 96-well plates at a density of 5000 cells per well and treated with different exosomes. After incubation for 0, 24, 48, and 72 h, 10 μL of CCK-8 reagent (Dojindo, Tokyo, Japan) was added to each well and incubated at 37°C for 2 h. The optional density (OD) of each well at 450 nm was detected by a modular multimode microplate reader (Bio Tek, USA).

EdU Assay

A549 cells were seeded in a 96-well plate at a density of 10,000 cells/well and treated with different exosomes. After 24 h, preheated EdU (10 μM final concentration in medium) was added to the culture medium and incubated for 2 h. The cells were fixed with 4% paraformaldehyde and then permeabilized with 0.5% Triton X-100 for 15 min. Then, the cells were stained using a Beyoclick™ EdU cell proliferation kit Alexa Fluor 647 (Beyotime, China) and imaged using ImageXpress Micro Confocal with MetaXpress software.

For lung explants, preheated EdU (10 μM final concentration in medium) was added to lung explants culture medium at 12 h prior to the 72 h endpoint of the experiments. For fetal lungs after intra-amniotic injection, EdU (150 μg/g concentration) were injected intraperitonally to pregnant mice at 12 h prior to the E18.5 endpoint of experiments. Samples were then fixed and processed for 4% paraformaldehyde, dehydrated and sectioned. The following Click-iT protocol was processed as stated above and imaged using ImageXpress Micro Confocal with MetaXpress software.

Flow Cytometry Analysis

A549 cells were seeded in a 6-well plate at a density of 200,000 cells/well and treated with different exosomes. The integrity of the cells was measured using an Annexin V-FITC/PI dual fluorescent staining kit (BD Biosciences, CA, USA) and quantified using flow cytometry according to the manufacturer's instructions. Briefly, the cells were harvested and washed with PBS, then resuspended in 500 μL of 1 x binding buffer to a concentration of 1×10^6 cells/mL. Subsequently, 5 μL of Annexin V-FITC and 10 μL of PI were added to the cells in order. After incubation at room temperature for 15 min in darkness, the stained cells were placed on ice and subjected to the Accuri C6 flow cytometer (BD Biosciences, CA, USA). Data acquisition and analysis were performed using BD software.

TUNEL Assay

Cell apoptosis experiments on lung explants and fetal lungs after intra-amniotic injection were conducted with the TUNEL assay for in situ apoptosis detection using a TUNEL BrightGreen Apoptosis Detection Kit (A112-01, Vazyme), according to the manufacturer's protocol. Quantification of the TUNEL signal was conducted with ImageXpress Micro Confocal with MetaXpress software.

qRT–PCR

The total RNA of the A549 cells, lung explants or fetal lung after intra-amniotic injection were extracted using TRIzol reagent (Tiangen, China) according to the manufacturer's instructions. Purified RNA was quantified using a NanoDrop-2000 spectrophotometer (Thermo Fisher Scientific). cDNA synthesis and PCR amplification were conducted using Evo M-MLV Mix Kit with gDNA Clean for qPCR (AG11728, Accurate Biotechnology) on an ABI 7500 Real-Time PCR system (Applied Biosystems, Waltham, MA, USA). The relative gene expression was expressed using the 2-ΔΔCT method with GAPDH serving as internal control. Primers were synthesized by Accurate Biotechnology (Hunan, China), and the primer sequences are shown in Table S2.

Histology and Immunofluorescence Staining

Fetal lungs after intra-amniotic injection were isolated and fixed in 4% paraformaldehyde at room temperature. For evaluation of the degree of lung alveolarization, paraffin sections (4-μm thickness) of the lung samples were chosen at

random and stained with haematoxylin and eosin (H&E) to assess the number of alveoli (the radial alveolar count, RAC) and the lung surface tissue density as previously described.[31]

Immunofluorescence staining was performed to assess the expression of lung explants and fetal lungs under different conditions. Briefly, 4 μm thick section of lung explants or fetal lungs were deparaffinized in xylene. Then, the tissues were hydrated in a series of concentrations of ethanol (100%, 95%, and 70%), 5 min per concentration, followed by three rounds of rinsing with PBS at room temperature. The antigen retrieval was performed by immersing the slides in EDTA antigen retrieval buffer (pH 8.0) and maintaining them at a sub-boiling temperature for 8 min, followed by standing for 8 min and incubation with another sub-boiling temperature for 7 min. Then, the tissues were blocked in 5% bovine serum albumin (BSA) solution for 30 min. The tissues were incubated with the anti-SPC antibody (ab211326, Abcam) for immunofluorescence at 4°C overnight. Subsequently, the fluorescent-dye (Alexa Fluor 555) conjugated secondary antibodies were incubated for 1 hour. After 3 washes with PBS, fluorescence images were taken using the ImageXpress Micro Confocal system with MetaXpress software. The protein expression was quantified using ImageJ software (NIH, MD, USA).

miRNA Sequencing Analysis

Total RNA was extracted from placenta-derived exosomes of normal and GDM umbilical cord blood plasma by using TRIzol (Invitrogen) according to the manufacturer's instructions. Small RNA libraries were constructed using the Illumina TruSeq Small RNA Preparation Kit according to Illumina's TruSeq Small RNA Sample Preparation Guide. The purified cDNA library was used for cluster generation on Illumina's Cluster Station and then sequenced on Illumina GAIIx, following the vendor's instrument operating instructions. ACGT101-miR v4.2 (LC Sciences) was used for sequencing data analysis. Briefly, raw reads were subjected to an in-house program, ACGT101-miR, to remove adapter dimers, junk, low complexity, common RNA families (rRNA, tRNA, snRNA, snoRNA), and repeats. Subsequently, unique sequences with a length of 18 to 26 bases were mapped to specific species precursors in miRBase 22.0 by BLAST search (Basic Local Alignment Search Tool) to identify known miRNAs and novel 3p- and 5p-derived miRNAs. The differentially expressed miRNAs identified on the basis of normalized deep-sequencing counts were analysed with the R package limma. Two computational target prediction algorithms (TargetScan50 [http://www.targetscan.org/vert_50/] and miRanda 3.3a [https://bioweb.pasteur.fr/packages/pack@miRanda@3.3a]) were used to identify miRNA binding sites. The data predicted by both algorithms were combined, and the overlaps were calculated. The Gene Ontology terms and KEGG pathways (Kyoto Encyclopedia of Genes and Genomes) of the most abundant miRNAs, and miRNA targets were also determined.

Statistical Analysis

Differences between two groups were compared using two-tailed Student's *t* test. A $p < 0.05$ was considered to be statistically significant. All statistical analyses were performed using GraphPad Prism software version 8.0.

Results

Isolation and Characterization of Exosomes

Exosomes derived from umbilical cord blood plasma and HTR-8/SVneo trophoblasts were successfully isolated according to modified protocols depicted in Figure 1A. Figure 1B shows the expression of specific exosomal biomarkers including CD63 and TSG101 and the placenta-specific biomarker PLAP. Compared with F1 grade, the expression of these proteins increased in a grade-dependent manner among F1-F3, then decreased and disappeared at F6 stage. The expression of CD63, TSG101, and PLAP of exosomes derived from HTR8/SVneo trophoblast were also determined in vitro shown in Figure 1C. The morphology of exosomes was determined by TEM analysis. As shown in Figure 1D, exosomes in all groups were found to be with typical cup-shaped morphologies and double-layered membrane structures. The nanoparticle tracking analysis revealed that the exosome was within the expected range of 30–200 nm. Compared with NUB group, the concentration of GDMUB-exos was higher (7.75e+10 ± 2.11e+09 particles/mL vs 3.00×10^{10} ± 3.91e+09 particles/mL), and HG-exos was higher than NC-exos (4.90e+10 ± 2.08e+09 particles/mL vs 1.08e+10 ± 1.30e+09 particles/mL) (Figure 1E).

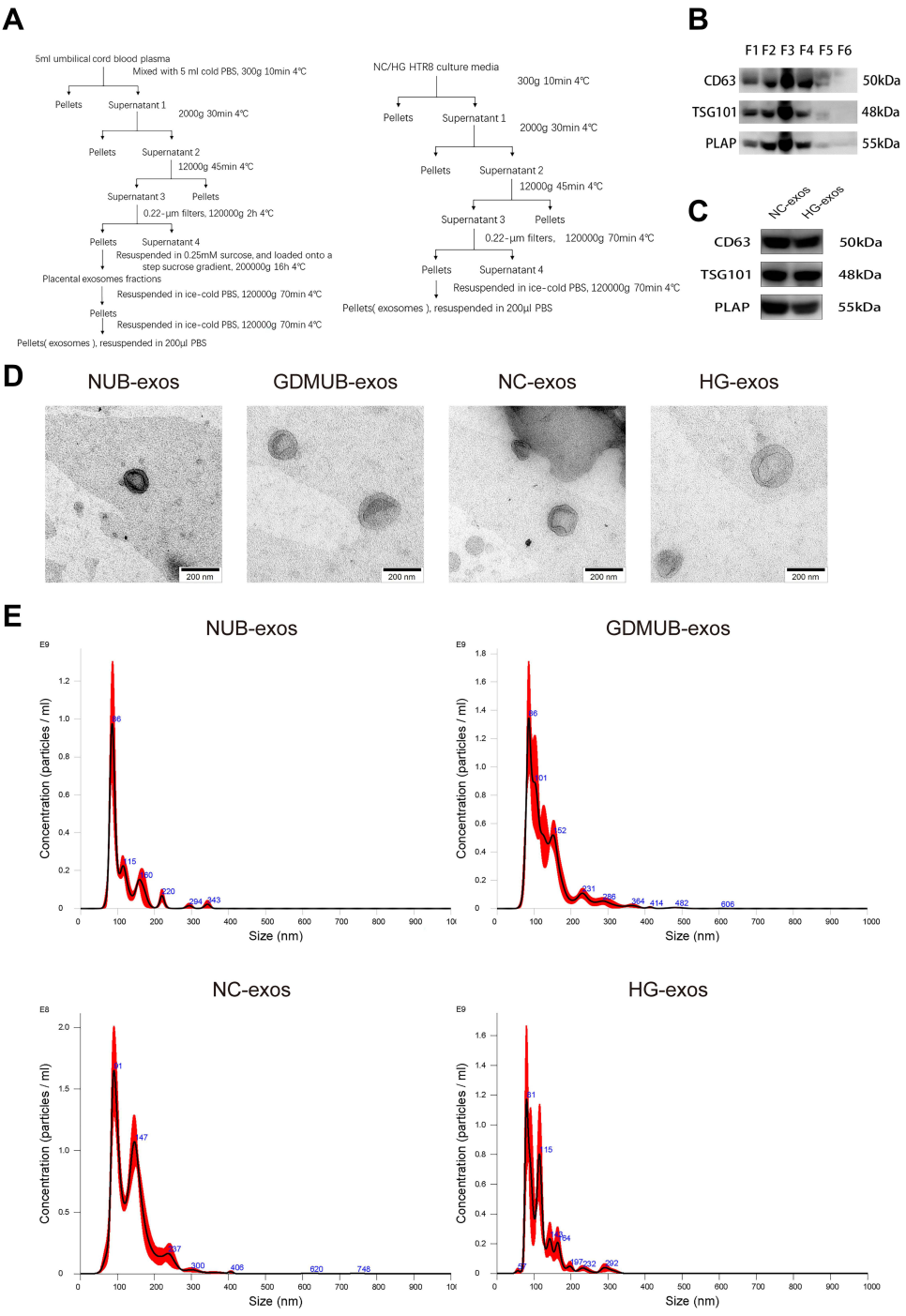

Figure 1 Characterization of exosomes derived from umbilical cord blood plasma and HTR8/SVneos cells. (**A**) Schematic diagrams for exosomes isolations from umbilical cord blood plasma and HTR8/SVneos cells culture media. (**B** and **C**) Expression of exosomal CD63, TSG101 and PLAP were examined by Western blot analysis. (**D**) The morphology of exosomes were captured by transmission electron microscopy (TEM). Scale bars, 200 μm. (**E**) The particle size and concentration were analyzed by nanoparticle tracking analysis (NTA).

miRNA Profiles Vary in GDM Pregnancies

The genome-wide miRNA expression was profiled to show the effect of GDM on the cargo of exosomal contents. As shown in Figure 2A, a total of 1885 miRNAs were identified, of which 61 miRNAs were differentially expressed (15 miRNAs upregulated and 46 miRNAs downregulated) (Figure 2B and C). The target genes of the differentially expressed miRNAs were predicted using TargetScan and miRanda. Then the main biological processes, cellular components, and

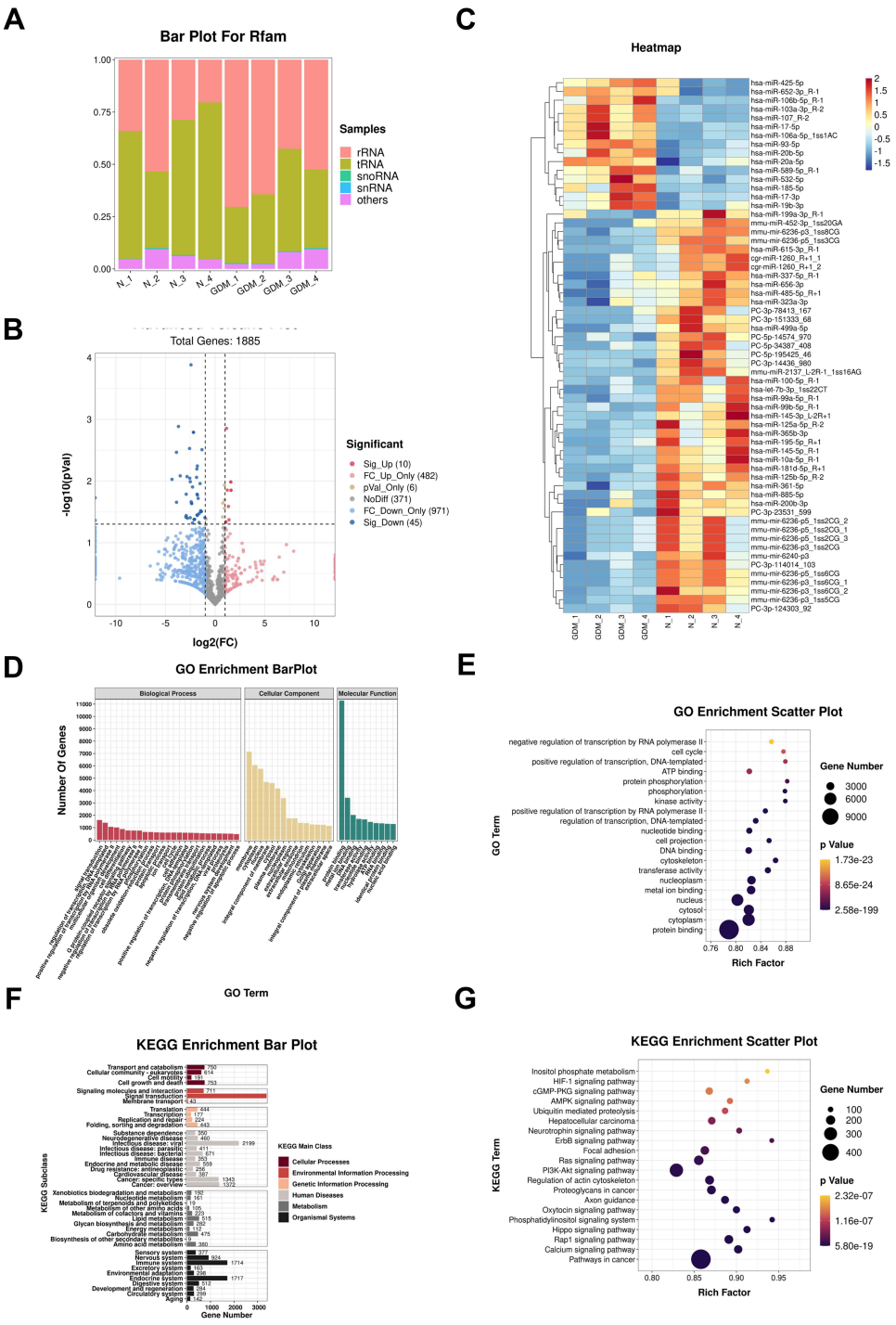

Figure 2 MiRNA sequencing analysis. (**A**) Bar chart representation of the distribution of small RNA categories in NUB-exo and GDMUB-exo samples. (**B** and **C**) Volcano plot and heatmap of differentially expressed miRNAs. (**D** and **E**) Bar plot and scatter plot of GO enrichment of the target genes. The rich factor indicates the ratio of the number of differentially expressed genes divided by the total number of genes annotated with a specific term. For a term, a smaller p value indicates a higher degree of enrichment. The diameter of the point represents the number of genes enriched with the item. (**F** and **G**) Bar plot and scatter plot of KEGG enrichment analysis of the target genes. The percentage of genes refers to the percentage of significantly enriched genes in the corresponding secondary categories. The number of target genes enriched in the KEGG pathway, p value and rich factor are shown in scatterplot. Rich factor = (number of target genes in KEGG pathway)/(total number of genes in KEGG pathway).

molecular functions determined by GO analysis are shown in Figure2D and E. To better reveal the significant biological pathways of the predicted target genes, we performed a KEGG pathway enrichment analysis. The top 20 statistically significantly enriched pathways are identified and are shown in Figure2F and G, which included the calcium signaling pathway, Rap1 signaling pathway, Hippo signaling pathway, PI3K-Akt signaling pathway etc.

GDM-Associated Exosome Treatment Disrupts A549 Cell Homeostasis and Suppresses Expression of Lung Surfactant Protein

To investigate the biological effects of GDM-associated exosomes on A459 cells, we stained the exosomes and A549 cells in different colors. As shown in Figure 3A, the PKH67-labeled exosomes were found to be internalized by A549 cells in all groups. Compared with cells treated with NUB-exos and NC-exos, cells in the GDMUB-exos and HG-exos groups showed an increased cell apoptosis rate as shown in Figure 3B and C. The CCK8 assay showed increased cell viability in a time-dependent manner in all groups, whilst the viability of NUB-exos and NC-exos-treated cells was higher in all time points than that of the GDMUB-exos and HG-exos treated cells (Figure 3D). In contrast with cell apoptosis assay, the EdU assay showed decreased cell proliferation rate in GDMUB-exos and HG-exos groups as compared to NUB-exos and NC-exos groups (Figure 3E and F). Also, the expression of apoptotic biomarkers such as BAX, BIM, and cleaved CASPASE-3 was upregulated in GDMUB-exos and HG-exos groups, while the anti-apoptotic protein BCL-2 was downregulated. Moreover, the expression of lung surfactant protein was detected as evidence of the effects of exosome exposure on lung development. As shown in Figure 3G-L, compared with the NUB-exos and NC-exos groups, the expression of lung surfactant protein A-D was downregulated after GDMUB-exos and HG-exos treatment both at transcriptional and post-transcriptional levels. These data indicate that umbilical cord blood plasma- and trophoblast-derived exosomes can be internalized by human lung epithelial cells, and intervention with GDM-associated exosomes causes human lung epithelial cell apoptosis and suppress cell viability and proliferation along with decreased expression of lung cell surfactant proteins.

GDM-Associated Exosome Treatment Impedes the Growth, Branching Morphogenesis, and Maturation of Fetal Lung Explants ex vivo

Noting the adverse effects of GDMUB-exos/HG-exos on A549 cells, we sought to explore the collective effects of GDMUB-exos/HG-exos on lung development. Using an ex vivo exosome exposure model of fetal lung explants, we observed the morphological alteration of lung explants and evaluated the expression of molecules involved in lung development. As shown in Figure 4A, compared with the control group, we found scattered PKH67-labeled exosomes over the observation fields in all four groups. After maintaining for 72 h, the growth and branching morphogenesis of GDMUB-exos and HG-exos treated lung explants were inhibited as compared to NUB-exos and NC-exos groups. The HG-exos group developed large, cyst-like structures at the distal tips (Figure 4B) and the number of terminal buds and the area of lung surfaces decreased and shrank in GDMUB-exos and HG-exos groups (Figure 4C and D). For lung physiological and functional evaluation, we detected the expression of lung surfactant protein and apoptotic biomarkers. As shown in Figure 4E-J, compared with NUB-exos and NC-exos groups, the expression of surfactant protein A-D was downregulated at both transcriptional and post transcriptional levels after GDMUB-exos and HG-exos treatments. Immunofluorescence assay also indicated that the expression of SPC was reduced in GDMUB-exos and HG-exos groups (Figure 4K and L). Also, the expression of Fgf10, Vegfa and its receptor Flt-1 and Kdr involved in fetal lung development was consistently downregulated in GDMUB-exos and HG-exos groups, whilst Sox9 was upregulated at translational level (Figure 4G and J). Meanwhile, the expression of apoptotic biomarkers such as BAX, BIM and cleaved CASPASE-3 was upregulated in GDMUB-exos and NG-exos groups, whilst the anti-apoptotic protein BCL-2 was downregulated (Figure 4E, F, H and I). Moreover, results of EdU assay and TUNEL assay confirmed the increased number of apoptotic cells and decreased number of proliferative cells in GDMUB-exos and HG-exos treated explants (Figure 4M-P). These data suggest that GDM-associated exosome can impede the growth, branching morphogenesis, and maturation of lung explants ex vivo.

GDM-Associated Exosome Treatment Retards Lung Development in vivo

To further investigate the effects of exosomes on fetal lung development in vivo, we applied different exosomes to pregnant C57BL/6J mice on E14.5 via intra-amniotic injections (Figure 5A). As shown in Figure S1, different PKH67-labelled exosomes could all be detected in lung cells. Figure 5B and C showed the fetuses and variation of fetal weight and CRL. Compared with NUB-exos and NC-exos groups, both indicators decreased in GDMUB-exos and HG-exos

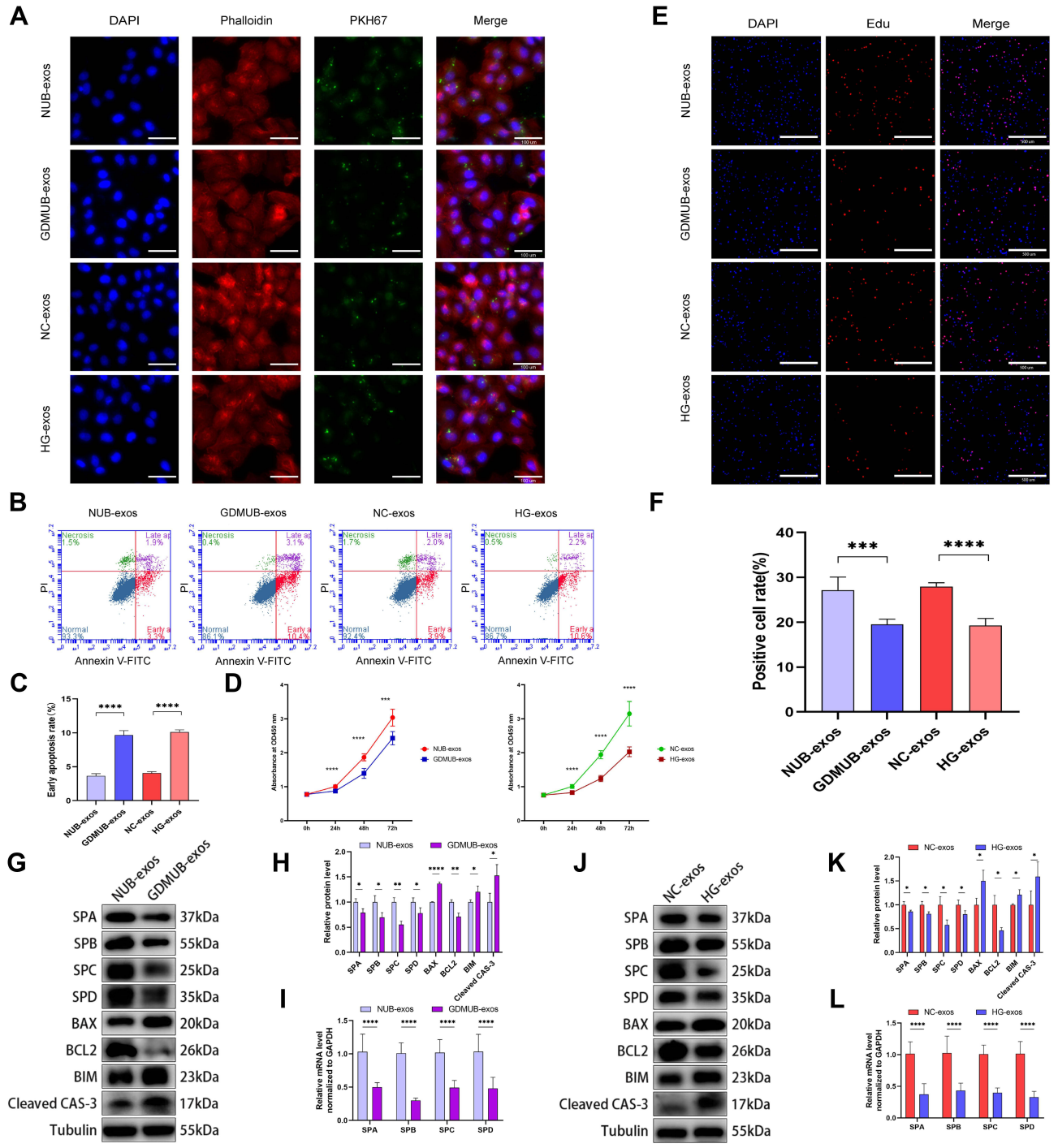

Figure 3 GDM-associated exosomes disrupted cell homeostasis and decreased the expression of lung surfactant proteins. (**A**) PKH67-labeled exosomes could be uptaken by A549 cells after incubated for 24h. Nuclei were counterstained with DAPI and the cytoskeleton was counterstained with phalloidin-iFluor 594. Scale bars, 100 μm. (**B–L**) A549 cells were treated with different groups exosomes (100 μg/mL) for 24 h. (**B** and **C**) The early apoptotic rate determined by flow cytometry analysis with annexin V and PI staining (n=5). (**D**) Cell viability analyzed by CCK8 assays (n=6). (**E** and **F**) Cell proliferation rate analyzed by EdU assays (n=6). Scale bars, 500 μm. (**G** and **H**) Western blot analysis of lung surfactant proteins A, B, C and D, BAX, BIM, BCL2, and cleaved CAS-3 expression in A549 cells treated with NUB-exos or GDMUB-exos for 24 h, quantified by signal intensity normalized to GAPDH (n=3). (**I**) Relative gene expression of lung surfactant proteins A, B, C, and D in the A549 cells treated with NUB-exos or GDMUB-exos for 24 h were measured by qRT–PCR (n=9). (**J** and **K**) Western blot analysis of lung surfactant proteins A, B, C, and D, BAX, BIM, BCL2, and cleaved CAS-3 expression in the A549 cells treated with NC-exos or HG-exos for 24 h, quantified by signal intensity normalized to GAPDH (n=3). (**L**) Relative gene expression of lung surfactant proteins A, B, C, and D in the A549 cells treated with NC-exos or HG-exos for 24 h was measured by qRT–PCR (n=9). *p < 0.05, **p < 0.01, ***p < 0.001, ****p < 0.0001.

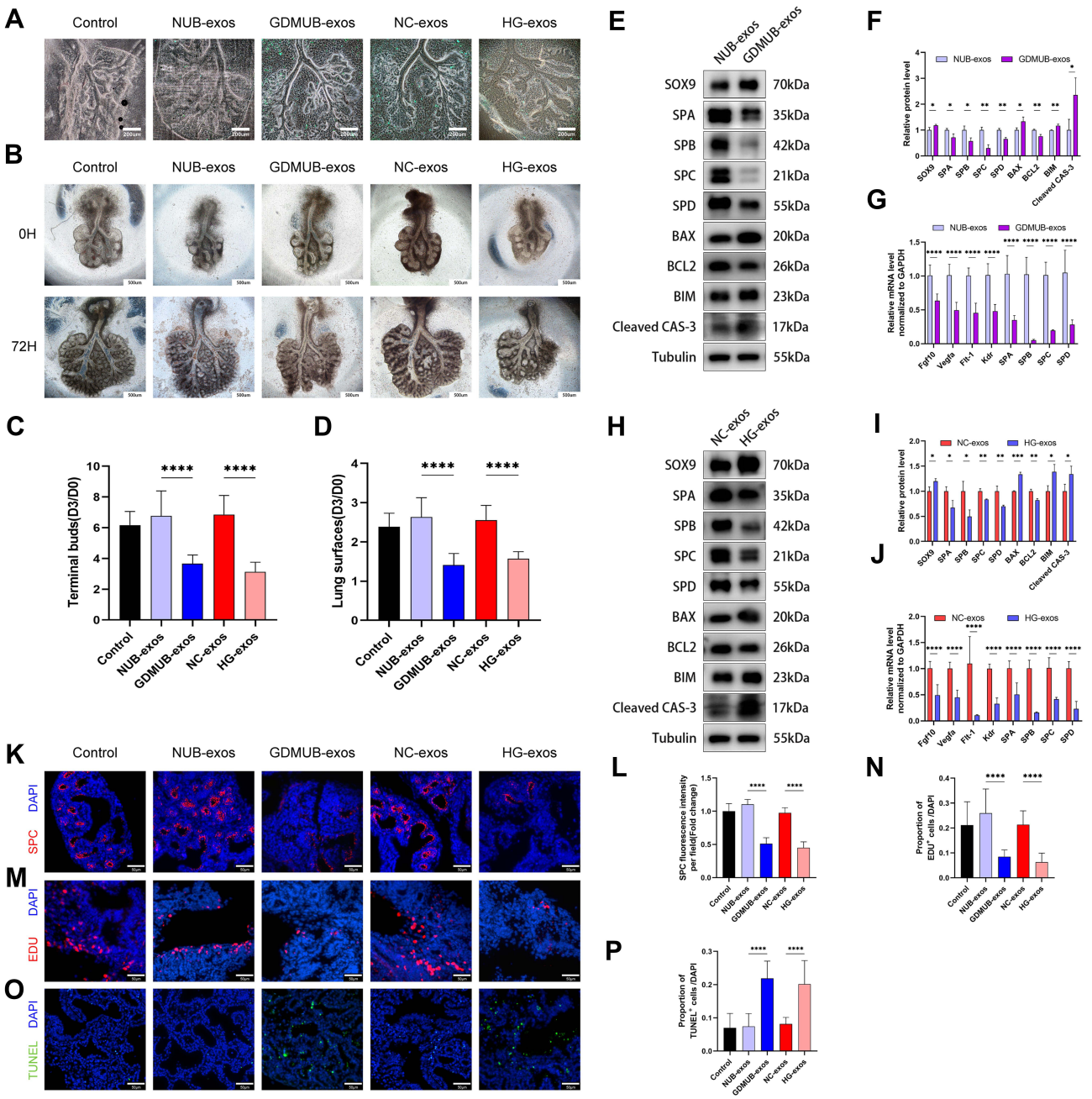

Figure 4 GDM-associated exosomes impeded the growth, branching morphogenesis and maturation of fetal lung explants. (**A**) PKH67-labeled exosomes could be detected in lung explants after incubated for 72 h. Scale bars, 200 μm. (**B–N**) The E11.5 lung explants treated with different groups exosomes (200μg/mL) for 72 h. (**B**) Representative images of E11.5 lung explants following 72 h ex vivo cultures with different groups exosomes. Scale bars, 500 μm. (**C** and **D**) Quantification of the number of terminal buds (n=12) and the area of lung explants surfaces (n=12) and expressed as the D3/D0 ratio. (**E** and **F**) Western blot analysis of lung surfactant protein A, B, C, and D, SOX9, BAX, BIM, BCL2, and cleaved CAS-3 expression in the lung explants treated with NUB-exos or GDMUB-exos for 72 h, quantified by signal intensity normalized to GAPDH (n=3). (**G**) Relative gene expression of lung surfactant proteins A, B, C, and D, the fibroblast growth factor 10 (Fgf10) and vascular endothelial growth factor (Vegfa) and its receptors (Flt1 and Kdr) in the lung explants treated with NUB-exos or GDMUB-exos for 72 h were measured by qRT–PCR (n=9). (**H** and **I**) Western blot analysis of lung surfactant protein A, B, C, and D, SOX9, BAX, BIM, BCL2, and cleaved CAS-3 expression in the lung explants treated with NC-exos or HG-exos for 72 h, quantified by signal intensity normalized to GAPDH (n=3). (**J**) Relative gene expression of lung surfactant proteins A, B, C, and D, the fibroblast growth factor 10 (Fgf10) and vascular endothelial growth factor (Vegfa) and its receptors (Flt1 and Kdr) in the lung explants treated with NUB-exos or GDMUB-exos for 72 h were measured by qRT–PCR (n=9). (**K** and **L**) Immunofluorescence experiments of lung surfactant protein C (SPC) in lung explants (SPC, green; DAPI nuclear stain, blue; scale bar, 50 μm), and quantified by immunofluorescence intensity (n≥10). (**M** and **N**) Images of EdU assays showed the proliferating cells of lung explants (EdU, red; DAPI nuclear stain, blue; scale bar 50 μm), quantified by the proportion of EdU+ cells (n≥7). (**O** and **P**) Images of TUNEL assay showed the apoptotic cells of lung explants (TUNEL, green; DAPI nuclear stain, blue; scale bar 50 μm), quantified by the proportion of TUNEL+ cells (n=12). *p < 0.05, **p < 0.01, ***p < 0.001, ****p < 0.0001.

https://doi.org/10.2147/IJN.S396194 DovePress

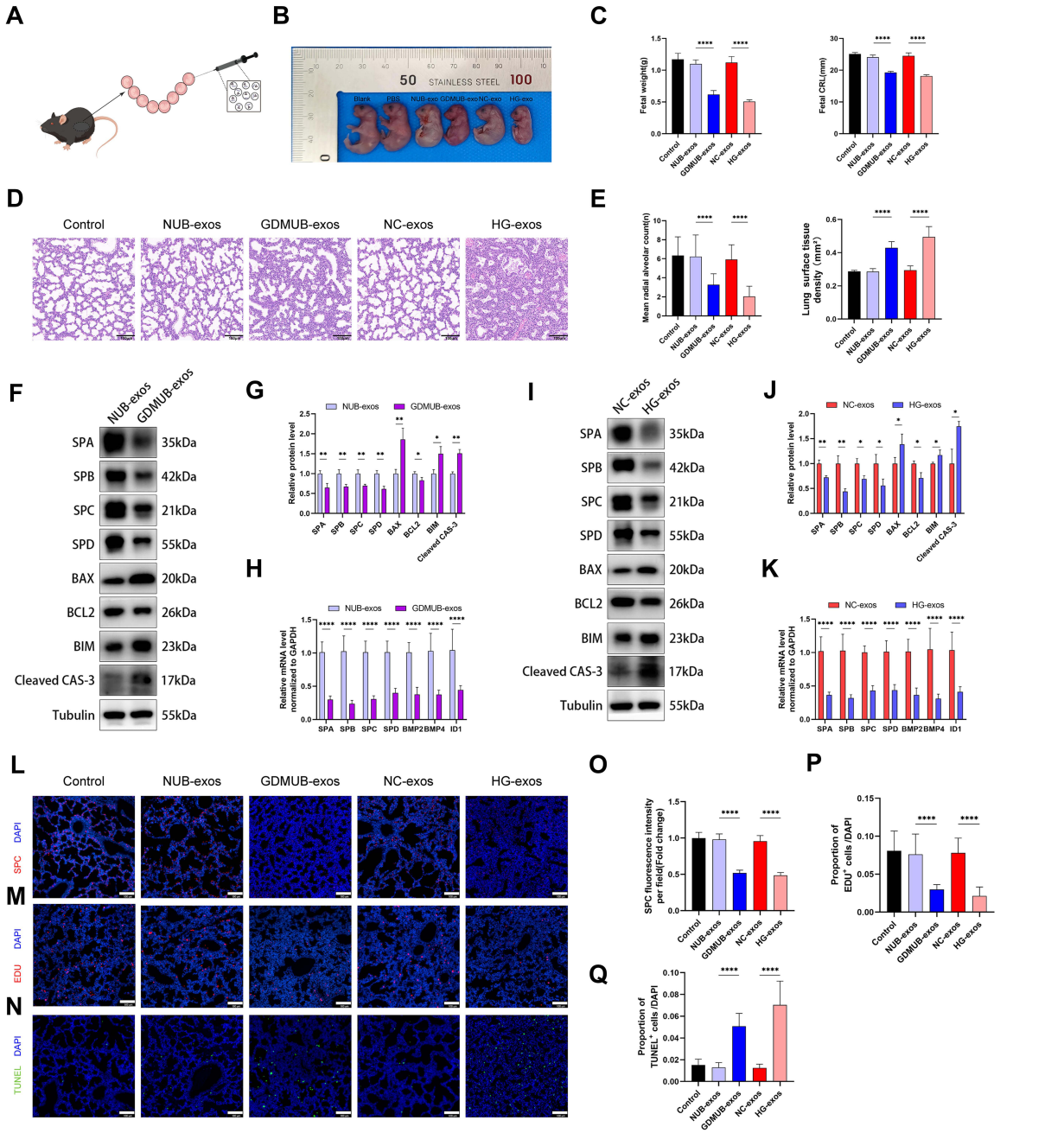

Figure 5 GDM-associated exosomes retarded the development of fetal lung in vivo. (**A**) Illustration of intra-amniotic injection of different groups exosomes on E14.5 (by Figdraw). (**B**) Representative images of fetuses harvested on E18.5 after intra-amniotic injection of exosomes from different groups on E14.5 (order from left to right: Blank, PBS (Control), NUB-exo, GDMUB-exo, NC-exo, HG-exo). (**C**) Quantification of fetal weight and fetal crown-rump length in different groups exosomes (n=10). (**D–Q**) The fetal lungs were harvested on E18.5 after intra-amniotic injection of different groups exosomes on E14.5. (**D**) Representative histology images (haematoxylin/eosin) of fetal lungs. Scale bar 100 μm. (**E**) Quantification of the number of alveoli (radial alveolar count, RAC) (n=26) and the area of lung surface tissue density (n=13). (**F** and **G**) Western blot analysis of lung surfactant protein A, B, C, and D, BAX, BIM, BCL2, and cleaved CAS-3 expression in fetal lungs harvested on E18.5 after intra-amniotic injection of NUB-exos or GDMUB-exos on E14.5, quantified by signal intensity normalized to GAPDH (n=3). (**H**) Relative gene expression of lung surfactant protein A, B, C, and D and BMP (bone morphogenetic protein) signalling (BMP2, BMP4, and Id1) in fetal lungs harvested on E18.5 after intra-amniotic injection of NUB-exos or GDMUB-exos on E14.5 was measured by qRT–PCR (n≥9). (**I** and **J**) Western blot analysis of lung surfactant protein A, B, C, and D, BAX, BIM, BCL2, and cleaved CAS-3 expression in fetal lungs harvested on E18.5 after intra-amniotic injection of NC-exos or HG-exos on E14.5, quantified by signal intensity normalized to GAPDH (n=3). (**K**) Relative gene expression of lung surfactant protein A, B, C, and D and BMP (bone morphogenetic protein) signalling (BMP2, BMP4, and Id1) in fetal lungs harvested on E18.5 after intra-amniotic injection of NC-exos or HG-exos on E14.5 was measured by qRT–PCR (n≥9) (**L** and **O**) Immunofluorescence experiments of lung surfactant protein C (SPC) in fetal lung (SPC, green; DAPI nuclear stain, blue; scale bar, 100 μm), and quantified by immunofluorescence intensity (n=25). (**M** and **Q**) Images of EdU assay showed the proliferating cells of fetal lungs (EdU, red; DAPI nuclear stain, blue; scale bar 100 μm), quantified by the proportion of EdU+ cells (n=13). (**N** and **R**) Images of TUNEL assay showed the apoptotic cells of fetal lungs (TUNEL, green; DAPI nuclear stain, blue; scale bar 100 μm), quantified by the proportion of TUNEL+ cells (n=20). *p < 0.05, **p < 0.01, ****p < 0.0001.

groups. Consistently, the radial alveolar count (RAC) decreased in NUB-exos and NC-exos groups, whilst the lung surface tissue density increased as shown in Figure 5D and E. Besides, the expression of the lung surfactant protein A-D of GDMUB-exos and HG-exos was downregulated at both transcriptional and post transcriptional levels as compared to the NUB-exos and NC-exos group (Figure 5F-K). Moreover, the immunofluorescence assay also indicated that the expression of SPC was reduced in GDMUB-exos and HG-exos groups (Figure 5L and O). The expression of several molecules related to lung maturation in bone morphogenetic protein (BMP) signalling (BMP2, BMP4 and Id1) were also downregulated in GDM-exos and HG-exos groups (Figure 5H and K). Additionally, the expression of apoptotic biomarkers such as BAX, BIM and cleaved CASPASE-3 was upregulated in GDMUB-exos and HG-exos groups, whilst the anti-apoptotic protein BCL-2 was downregulated (Figure 5F, G, I and J). Results of EdU assay and TUNEL assay confirmed the increased number of apoptotic cells and decreased number of proliferative cells in GDMUB-exos and HG-exos treated groups (Figure 5M, N, P and Q). These data suggest that GDM exosomes can retard fetal lung development and maturation in vivo.

Discussion

Since the "Barker hypothesis" was proposed in the 1990s,[32] more and more studies report that the events in fetal period may contribute to the later onset of cardiovascular diseases or diabetes in adults.[33–35] With the increase of chronic lung diseases of GDM neonatal in early childhood,[36] the fetal lung development has attracted our attention. Placenta is believed to be the determinant role of the maternal-fetal interface, and its structure and function are crucial to fetal development and health.[37] Accumulating evidence has proved that the placenta as a selective barrier, makes adaptive changes to environmental and maternal factors, and is involved in programming offspring health.[38] It has been reported that pro-inflammatory responses and increased apoptotic rates in trophoblasts,[39] increased trophoblast oxidative/nitrative stress,[40] and reduced trophoblast mitochondrial respiration[41,42] are related to the pathogenesis of GDM, which would lead to trophoblast dysfunction, impaired placenta development, restricted fetal growth, stillbirth,[43] and neonatal respiratory distress syndrome.[44] Besides, in a mouse model, a previous study also demonstrated that exposure of pregnant mice to a diet high in fat (HFD) would cause placental inflammation, resulting in placental insufficiency, fetal growth restriction (FGR), and inhibition of fetal lung development,[45] which suggests that placental inflammation may affect lung development. However, the effects of dysregulated placentas on fetal lung development in GDM have not been fully elucidated yet.

Exosomes have emerged as important transporters involved in signal transmission and cell-to-cell communication. Placenta-derived exosomes have been reported to play an important role in the maternal–fetal interface in normal and complicated pregnancies.[46] During pregnancy, placenta-derived exosomes can be identified as early as 6 weeks of gestation,[47] and are differentiated from other exosomes by positively expressing placental alkaline phosphatase (PLAP) proteins.[48] Several studies reported that placenta-derived exosomes can modulate maternal immune tolerance by acting on the NK cell receptor NKG2D[49] or reprogramming circulating monocytes[50] to achieve a successful pregnancy. In preeclampsia, the expression of miR-155 is increased in placenta-derived exosomes of maternal serum, and the exosomes inhibit eNOS expression in endothelial cells, which promotes the development of PE.[51] Placenta-derived exosomal miRNAs from GDM can weaken insulin sensitivity and decrease glucose uptake in skeletal muscles.[23]

In the present study, to the best of our knowledge, we are the first to isolate and characterize the placenta-derived exosomes in normal and GDM umbilical cord blood plasma (NUB-exos and GDMUB-exos) and provide fresh evidence that the placenta-derived exosomes in GDM umbilical cord blood plasma can adversely affect the normal development of fetal lung by establishing in vitro, ex vivo and in vivo exosome exposure models. Placenta-derived exosomes are a heterogeneous group of exosomes secreted by various placental cells, and most of them are released by the syncytiotrophoblastic layer.[47,52] Therefore, we cultured human trophoblast HTR-8/SVneo cells with D-glucose (5 mM or 25 mM) for 48 h and isolated the exosomes (NC-exos and HG-exos) in conditioned media to further confirm the adverse effects of trophoblasts on lung development.

It is not ethically acceptable to obtain human lung tissues from GDM fetuses or neonatal babies. In this way, we applied three different models to investigate the role of GDMUB-exos in fetal lung development collectively. For the in vitro assay, we chose the human alveolar type II A549 cell line to use as a model of alveolar epithelial type II cells.

The A549 cells are demonstrated with typical morphology and ultrastructural features, such as the lamellar body responsible for pulmonary surfactant protein synthesis and release.[53–55] For ex vivo assay, we dissected the E11.5 fetal lung explants of mice and the following pseudoglandular stage (E12.5-E16.5) was the crucial stage during branching morphogenesis which could form almost all of the future airways.[56] For in vivo assay, we performed intra-amniotic injection on E14.5, and evaluated the fetal lung at the saccular stage (E18.5), which contributes to the distinguishment of different lung development stages.[56]

Fetal lung development is a highly regulated and well-orchestrated process. Branching morphogenesis comprises fine spatiotemporal regulation of molecular pathways among epithelial cells, mesenchymal cells and the extracellular matrix.[57,58] Normal cell proliferation and apoptosis play an important role in perinatal and postnatal lung development.[59] The results of different internal or external environmental exposures may be different from each other. A study of chorioamnionitis stillborn lung histopathology revealed that chorioamnionitis induced apoptosis of distal airway epithelial cells and interfered with the normal proliferative activity.[60] Reina S Mayor found that maternal high-fat diet was associated with elevations in maternal glucose and insulin levels and reduced fetal lung cell proliferation compared with control fetal lungs.[45] In STZ-induced diabetic rats, TUNEL-positive cells which were mainly located at alveolar walls were significantly increased at birth and PCNA-positive cells which were located more in alveolar septa were also increased. However, another STZ-induced diabetic mouse study suggested that hyperglycemia increased pulmonary cell proliferation and decreased apoptosis.[61] Our study indicated that GDMUB-exos and HG-exos significantly inhibited lung cell proliferation and promoted apoptosis which disturbed the imbalance between lung cell proliferation and apoptosis and resulted in impaired fetal lung development.

In addition, epithelial cell differentiation is essential for branching morphogenesis and lung development. During mouse lung organogenesis, lung specification begins at E9.5 with the transformation of the foregut into the two lung buds and the separation of the trachea and oesophagus. Following a series of morphogenetic events, a final complex lung branchial tree develops.[62] Various signalling pathways and transcription factors are known to play roles in branching morphogenesis. Sox9 is a marker of distal epithelial progenitor cells. Briana E. Rockich et al demonstrated that epithelial-specific loss and gain of Sox9 caused severe branching defects in the lung, which developed large, cyst-like structures at the distal epithelial branch tips at all developmental times examined.[63] Moreover, with lung bud growth, Sox9+ progenitor cells gradually extended to distal portions stimulated by FGF10 secreted by mesenchymal cells.[64] In our ex vivo study, we found that after exposure to GDMUB-exos or HG-exos, the terminal buds and superficial areas of lung explants decreased, and the terminal buds developed large, cyst-like structures. Moreover, the expression levels of Sox9 were higher while Fgf10 were lower than those in the normal control groups evaluated by WB and qPCR, respectively. In addition, in our in vivo assays, we found that at E18.5, fetal lungs exposed to GDMUB-exos or HG-exos showed lung morphology more comparable to that at E14.5–15.5, suggesting that GDMUB-exos or HG-exos result in delayed structural lung development.

Besides the defective structural maturation, we sought to explore the changes in biological maturation of fetal lung underdevelopment. Lung surfactant protein is critical for lung development which can decrease the alveolar surface tension to increase lung compliance and prevent alveolar collapse at the end of expiration.[65] Previous studies have demonstrated that there was a significant reduction in the expression of surfactant proteins A, B and C in STZ-induced diabetic offspring.[66,67] Miakotina, O. L et al also found that the expression levels of SPA and SPB were inhibited by insulin in H441 cell lines.[68] Another previous ex vivo study suggested that the production of surfactant proteins B and C was significantly reduced with increased glucose concentrations of 100 mM (<10%) compared to 10 mM. However, surfactant protein A was not significantly affected by various levels of glucose.[69] Our study demonstrated that the GDMUB-exos and HG-exos could significantly reduce the expression of all kinds of surfactant proteins at the protein and mRNA levels via in vitro, ex vivo and in vivo models. Additionally, SPC immunofluorescence assays and the significantly reduced mRNA expression of BMP2, BMP4 and ID1 further proved our hypothesis.

Our miRNA sequencing results demonstrated that GDM significantly affected the miRNA contents of placenta-derived exosomes when compared to normal pregnancy. In our study, we found that miR-93-5p, miR-103/107, miR-17/106a, miR-20a, miR-185-5p, miR-19b-3p and so on were upregulated, while let-7b-3p, miR-99a, miR-125a/b, miR-145, miR-195-5p, miR-200b, and so on were downregulated; these molecules had high reads and significant p values in

GDMUB-exos compared to NUB-exos. The differentially expressed miRNAs in our study have been reported to be closely related to the pathogenesis of GDM and the fetal lung development. MiR-16-5p, miR-17-5p, miR-19a-3p, miR-19b-3p and miR-20a-5p were previously confirmed to be associated with insulin resistance and abnormal pregnancies.[70] Trajkovski M et al further demonstrated that the gain of miR-103/107 impaired glucose homeostasis and insulin sensitivity.[71] In addition, downregulated miR-125b and upregulated miR-144 were consistently dysregulated in circulating exosomes and the placenta from GDM-complicated pregnancies and were supposed to be of great diagnostic value.[72]

However, there are some limitations in the present study. First, the isolated placenta-derived exosomes from umbilical cord blood plasma were not pure. The methods used thus far in various studies, including ours, could only obtain exosome-enriched preparations, and we could not obtain the placenta-specific exosomes. In this way, more specific isolation methods are urgently needed. Second, the time point at which we collect umbilical cord blood was almost at birth, and we were not able to evaluate the different stages of lung development by using exosomes matched for gestational age for ethical reasons. Experiments with animal models may address this limitation. Besides, the differentially expressed miRNAs need to be further validated with more samples and the downstream signalling pathways involved in fetal lung development should be explored in future studies.

In conclusion, this paper provides sufficient evidence that placenta-derived exosomes exist in umbilical cord blood plasma, and all exosomes can be transferred into fetal lung and internalized by lung cells. We are the first to demonstrate that the adverse effect of placenta-derived exosomes from GDM umbilical cord blood plasma of on fetal lung cell proliferation, type II pneumocyte differentiation, and lung maturation via in vitro, ex vivo and in vivo models, which are associated with impaired fetal lung development and progressed to acute respiratory distress syndrome in neonates and early childhood. These data highlight an emerging role of placenta-derived exosomes in the pathogenesis of fetal lung underdevelopment in GDM pregnancies, and provide a novel strategy for maternal–fetal communication.

Disclosure

The authors report no conflicts of interest in this work.

References

1. Hod M, Kapur A, Sacks DA, et al. The International Federation of Gynecology and Obstetrics (FIGO) Initiative on gestational diabetes mellitus: a pragmatic guide for diagnosis, management, and care. *Int J Gynaecol Obstet*. 2015;131(Suppl 3):S173–211. doi:10.1016/S0020-7292(15)30007-2
2. McIntyre HD, Zhang C, Desoye G, et al. Gestational diabetes mellitus. *Nat Rev Dis Primers*. 2019;5:47. doi:10.1038/s41572-019-0098-8
3. Group, H. S. C. R. The Hyperglycemia and Adverse Pregnancy Outcome (HAPO) Study. *Int J Gynaecol Obstet*. 2002;78:69–77. doi:10.1016/s0020-7292(02)00092-9
4. Aboughalia H, Pathak P, Basavalingu D, et al. Imaging review of obstetric sequelae of maternal diabetes mellitus. *Radiographics*. 2022;42:302–319. doi:10.1148/rg.210164
5. Ejdesjo A, Wentzel P, Eriksson UJ. Influence of maternal metabolism and parental genetics on fetal maldevelopment in diabetic rat pregnancy. *Am J Physiol Endocrinol Metab*. 2012;302:E1198–1209. doi:10.1152/ajpendo.00661.2011
6. Gheorman L, Iliescu D, Ceausu I, et al. Importance of early complex evaluation in high-risk pregnancy associated to diabetes mellitus. Case presentation and review of the literature. *Rom J Morphol Embryol*. 2011;52:1127–1132.
7. Fung GP, Chan LM, Ho YC, et al. Does gestational diabetes mellitus affect respiratory outcome in late-preterm infants? *Early Hum Dev*. 2014;90:527–530. doi:10.1016/j.earlhumdev.2014.04.006
8. Abu-Heija AT, Al-Bash M, Mathew M. Gestational and pregestational diabetes mellitus in Omani women: comparison of obstetric and perinatal outcomes. *Sultan Qaboos Univ Med J*. 2015;15:e496–500. doi:10.18295/squmj.2015.15.04.009
9. Becquet O, Khabbaz F, Alberti C, et al. Insulin treatment of maternal diabetes mellitus and respiratory outcome in late-preterm and term singletons. *BMJ Open*. 2015;5:e008192. doi:10.1136/bmjopen-2015-008192
10. Delaney C, Cornfield DN. Risk factors for persistent pulmonary hypertension of the newborn. *Pulm Circ*. 2012;2:15–20. doi:10.4103/2045-8932.94818
11. Yildiz Atar H, Baatz JE, Ryan RM. Molecular mechanisms of maternal diabetes effects on fetal and neonatal surfactant. *Children*. 2021;8. doi:10.3390/children8040281
12. Raikkonen K, Gissler M, Kajantie E. Associations between maternal antenatal corticosteroid treatment and mental and behavioral disorders in children. *JAMA*. 2020;323:1924–1933. doi:10.1001/jama.2020.3937
13. Raikkonen K, Gissler M, Tapiainen T, Kajantie E. Associations between maternal antenatal corticosteroid treatment and psychological developmental and neurosensory disorders in children. *JAMA Netw Open*. 2022;5:e2228518. doi:10.1001/jamanetworkopen.2022.28518
14. Olmos-Ortiz A, Flores-Espinosa P, Díaz L, et al. Immunoendocrine dysregulation during gestational diabetes mellitus: the central role of the placenta. *Int J Mol Sci*. 2021;22. doi:10.3390/ijms22158087
15. Radaelli T, Varastehpour A, Catalano P, Hauguel-de Mouzon S. Gestational diabetes induces placental genes for chronic stress and inflammatory pathways. *Diabetes*. 2003;52:2951–2958. doi:10.2337/diabetes.52.12.2951
16. Taglauer E, Abman SH, Keller RL. Recent advances in antenatal factors predisposing to bronchopulmonary dysplasia. *Semin Perinatol*. 2018;42:413–424. doi:10.1053/j.semperi.2018.09.002

17. Parsons A, Netsanet A, Seedorf GJ, Abman SH, Taglauer ES. Understanding the role of placental pathophysiology in the development of bronchopulmonary dysplasia (BPD). *Am J Physiol Lung Cell Mol Physiol*. 2022. doi:10.1152/ajplung.00204.2022
18. Chiarello DI, Salsoso R, Toledo F, et al. Foetoplacental communication via extracellular vesicles in normal pregnancy and preeclampsia. *Mol Aspects Med*. 2018;60:69–80. doi:10.1016/j.mam.2017.12.002
19. Zhang Y, Liu Y, Liu H, Tang WH. Exosomes: biogenesis, biologic function and clinical potential. *Cell Biosci*. 2019;9:19. doi:10.1186/s13578-019-0282-2
20. Salomon C, Scholz-Romero K, Sarker S, et al. Gestational diabetes mellitus is associated with changes in the concentration and bioactivity of placenta-derived exosomes in maternal circulation across gestation. *Diabetes*. 2016;65:598–609. doi:10.2337/db15-0966
21. Rice GE, Scholz-Romero K, Sweeney E, et al. The effect of glucose on the release and bioactivity of exosomes from first trimester trophoblast cells. *J Clin Endocrinol Metab*. 2015;100:E1280–1288. doi:10.1210/jc.2015-2270
22. Salomon C, Torres MJ, Kobayashi M, et al. A gestational profile of placental exosomes in maternal plasma and their effects on endothelial cell migration. *PLoS One*. 2014;9:e98667. doi:10.1371/journal.pone.0098667
23. Nair S, Jayabalan N, Guanzon D, et al. Human placental exosomes in gestational diabetes mellitus carry a specific set of miRNAs associated with skeletal muscle insulin sensitivity. *Clin Sci (Lond)*. 2018;132:2451–2467. doi:10.1042/CS20180487
24. Valadi H, Ekstrom K, Bossios A, et al. Exosome-mediated transfer of mRNAs and microRNAs is a novel mechanism of genetic exchange between cells. *Nat Cell Biol*. 2007;9:654–659. doi:10.1038/ncb1596
25. Chen X, Liang H, Zhang J, Zen K, Zhang CY. Secreted microRNAs: a new form of intercellular communication. *Trends Cell Biol*. 2012;22:125–132. doi:10.1016/j.tcb.2011.12.001
26. Metzger B. International association of diabetes and pregnancy study groups recommendations on the diagnosis and classification of hyperglycemia in pregnancy. *Diabetes Care*. 2010;33:676–682. doi:10.2337/dc09-1848
27. Shen L, Li Y, Li R, et al. Placenta-associated serum exosomal miR-155 derived from patients with preeclampsia inhibits eNOS expression in human umbilical vein endothelial cells. *Int J Mol Med*. 2018;41:1731–1739. doi:10.3892/ijmm.2018.3367
28. Zhu J, Liu B, Wang Z, et al. Exosomes from nicotine-stimulated macrophages accelerate atherosclerosis through miR-21-3p/PTEN-mediated VSMC migration and proliferation. *Theranostics*. 2019;9:6901–6919. doi:10.7150/thno.37357
29. Nair S, Jayabalan N, Guanzon D, et al. Human placental exosomes in gestational diabetes mellitus carry a specific set of miRNAs associated with skeletal muscle insulin sensitivity. *Clin sci*. 2018;132:2451–2467. doi:10.1042/cs20180487
30. Del Moral PM, Warburton D. Explant culture of mouse embryonic whole lung, isolated epithelium, or mesenchyme under chemically defined conditions as a system to evaluate the molecular mechanism of branching morphogenesis and cellular differentiation. *Methods Mol Biol*. 2010;633:71–79. doi:10.1007/978-1-59745-019-5_5
31. Khoshgoo N, Kholdebarin R, Pereira-Terra P, et al. Prenatal microRNA miR-200b Therapy Improves Nitrofen-induced Pulmonary Hypoplasia Associated With Congenital Diaphragmatic Hernia. *Ann Surg*. 2019;269:979–987. doi:10.1097/SLA.0000000000002595
32. Barker DJ. Fetal nutrition and cardiovascular disease in adult life. *Lancet*. 1993;341:938–941. doi:10.1016/0140-6736(93)91224-a
33. Mestan KK, Steinhorn RH. Fetal origins of neonatal lung disease: understanding the pathogenesis of bronchopulmonary dysplasia. *Am J Physiol Lung Cell Mol Physiol*. 2011;301:L858–859. doi:10.1152/ajplung.00314.2011
34. Xita N, Tsatsoulis A. Fetal origins of the metabolic syndrome. *Ann N Y Acad Sci*. 2010;1205:148–155. doi:10.1111/j.1749-6632.2010.05658.x
35. Zou K, Ding G, Huang H. Advances in research into gamete and embryo-fetal origins of adult diseases. *Sci China Life Sci*. 2019;62:360–368. doi:10.1007/s11427-018-9427-4
36. Azad MB, Moyce BL, Guillemette L, et al. Diabetes in pregnancy and lung health in offspring: developmental origins of respiratory disease. *Paediatr Respir Rev*. 2017;21:19–26. doi:10.1016/j.prrv.2016.08.007
37. Burton GJ, Fowden AL, Thornburg KL. Placental origins of chronic disease. *Physiol Rev*. 2016;96:1509–1565. doi:10.1152/physrev.00029.2015
38. Cleal JK, Poore KR, Lewis RM. The placental exposome, placental epigenetic adaptations and lifelong cardio-metabolic health. *Mol Aspects Med*. 2022;87:101095. doi:10.1016/j.mam.2022.101095
39. Nguyen-Ngo C, Jayabalan N, Salomon C, Lappas M. Molecular pathways disrupted by gestational diabetes mellitus. *J Mol Endocrinol*. 2019;63:R51–R72. doi:10.1530/JME-18-0274
40. Lappas M, Hiden U, Desoye G, et al. The role of oxidative stress in the pathophysiology of gestational diabetes mellitus. *Antioxid Redox Signal*. 2011;15:3061–3100. doi:10.1089/ars.2010.3765
41. Hebert JF, Myatt L. Placental mitochondrial dysfunction with metabolic diseases: therapeutic approaches. *Biochim Biophys Acta Mol Basis Dis*. 2021;1867:165967. doi:10.1016/j.bbadis.2020.165967
42. Sobrevia L, Valero P, Grismaldo A, et al. Mitochondrial dysfunction in the fetoplacental unit in gestational diabetes mellitus. *Biochim Biophys Acta Mol Basis Dis*. 2020;1866:165948. doi:10.1016/j.bbadis.2020.165948
43. Bedell S, Hutson J, de Vrijer B, Eastabrook G. Effects of maternal obesity and gestational diabetes mellitus on the placenta: current knowledge and targets for therapeutic interventions. *Curr Vasc Pharmacol*. 2021;19:176–192. doi:10.2174/1570161118666200616144512
44. American College of Obstetricians and Gynecologists. ACOG Practice Bulletin No. 190: gestational Diabetes Mellitus. *Obstet Gynecol*. 2018;131:e49–e64. doi:10.1097/AOG.0000000000002501
45. Mayor RS, Finch KE, Zehr J, et al. Maternal high-fat diet is associated with impaired fetal lung development. *Am J Physiol Lung Cell Mol Physiol*. 2015;309:L360–368. doi:10.1152/ajplung.00105.2015
46. Mitchell MD, Peiris HN, Kobayashi M, et al. Placental exosomes in normal and complicated pregnancy. *Am J Obstet Gynecol*. 2015;213:S173–181. doi:10.1016/j.ajog.2015.07.001
47. Sarker S, Scholz-Romero K, Perez A, et al. Placenta-derived exosomes continuously increase in maternal circulation over the first trimester of pregnancy. *J Transl Med*. 2014;12:204. doi:10.1186/1479-5876-12-204
48. Kam W, Clauser E, Kim YS, Kan YW, Rutter WJ. Cloning, sequencing, and chromosomal localization of human term placental alkaline phosphatase cDNA. *Proc Natl Acad Sci U S A*. 1985;82:8715–8719. doi:10.1073/pnas.82.24.8715
49. Mincheva-Nilsson L, Nagaeva O, Chen T, et al. Placenta-derived soluble MHC class I chain-related molecules down-regulate NKG2D receptor on peripheral blood mononuclear cells during human pregnancy: a possible novel immune escape mechanism for fetal survival. *J Immunol*. 2006;176:3585–3592. doi:10.4049/jimmunol.176.6.3585
50. Bai K, Liu X, Li J, et al. Human placental exosomes induce maternal systemic immune tolerance by reprogramming circulating monocytes. *J Nanobiotechnology*. 2022;20:86. doi:10.1186/s12951-022-01283-2

51. Shen L, Vanhara P, Koutna I, et al. Placenta associated serum exosomal miR155 derived from patients with preeclampsia inhibits eNOS expression in human umbilical vein endothelial cells. *Int J Mol Med*. 2018;41:1731–1739. doi:10.3892/ijmm.2018.3367
52. Guarino E, Poggi C, Grieco GE, et al. Circulating MicroRNAs as biomarkers of gestational diabetes mellitus: updates and perspectives. *Int J Endocrinol*. 2018;2018:6380463. doi:10.1155/2018/6380463
53. Cooper JR, Abdullatif MB, Burnett E, et al. Long term culture of the A549 cancer cell line promotes multilamellar body formation and differentiation towards an alveolar Type II pneumocyte phenotype. *PLoS One*. 2016;11:e0164438. doi:10.1371/journal.pone.0164438
54. Rucka Z, Vanhara P, Koutna I, et al. Differential effects of insulin and dexamethasone on pulmonary surfactant-associated genes and proteins in A549 and H441 cells and lung tissue. *Int J Mol Med*. 2013;32:211–218. doi:10.3892/ijmm.2013.1363
55. Foster KA, Oster CG, Mayer MM, Avery ML, Audus KL. Characterization of the A549 cell line as a type II pulmonary epithelial cell model for drug metabolism. *Exp Cell Res*. 1998;243:359–366. doi:10.1006/excr.1998.4172
56. Schittny JC. Development of the lung. *Cell Tissue Res*. 2017;367:427–444. doi:10.1007/s00441-016-2545-0
57. Danopoulos S, Alonso I, Thornton ME, et al. Human lung branching morphogenesis is orchestrated by the spatiotemporal distribution of ACTA2, SOX2, and SOX9. *Am J Physiol Lung Cell Mol Physiol*. 2018;314:L144–L149. doi:10.1152/ajplung.00379.2017
58. Kimura J, Deutsch GH. Key mechanisms of early lung development. *Pediatr Dev Pathol*. 2007;10:335–347. doi:10.2350/07-06-0290.1
59. Del Riccio V, van Tuyl M, Post M. Apoptosis in lung development and neonatal lung injury. *Pediatr Res*. 2004;55:183–189. doi:10.1203/01.PDR.0000103930.93849.B2
60. May M, Marx A, Seidenspinner S, Speer CP. Apoptosis and proliferation in lungs of human fetuses exposed to chorioamnionitis. *Histopathology*. 2004;45:283–290. doi:10.1111/j.1365-2559.2004.01936.x
61. He MY, Wang G, Han SS, et al. Negative impact of hyperglycaemia on mouse alveolar development. *Cell Cycle*. 2018;17:80–91. doi:10.1080/15384101.2017.1403683
62. Metzger RJ, Klein OD, Martin GR, Krasnow MA. The branching programme of mouse lung development. *Nature*. 2008;453:745–750. doi:10.1038/nature07005
63. Rockich BE, Hrycaj SM, Shih H, et al. Sox9 plays multiple roles in the lung epithelium during branching morphogenesis. *Proc Natl Acad Sci U S A*. 2013;110:E4456–4464. doi:10.1073/pnas.1311847110
64. Park WY, Miranda B, Lebeche D, Hashimoto G. FGF-10 is a chemotactic factor for distal epithelial buds during lung development. *Dev Biol*. 1998;201:125–134. doi:10.1006/dbio.1998.8994
65. Veldhuizen EJ, Haagsman HP. Role of pulmonary surfactant components in surface film formation and dynamics. *Biochim Biophys Acta*. 2000;1467:255–270. doi:10.1016/s0005-2736(00)00256-x
66. Guttentag SH, Phelps DS, Stenzel W, Warshaw JB, Floros J. Surfactant protein A expression is delayed in fetuses of streptozotocin-treated rats. *Am J Physiol*. 1992;262:L489–494. doi:10.1152/ajplung.1992.262.4.L489
67. Guttentag SH, Phelps DS, Warshaw JB, Floros J. Delayed hydrophobic surfactant protein (SP-B, SP-C) expression in fetuses of streptozotocin-treated rats. *Am J Respir Cell Mol Biol*. 1992;7:190–197. doi:10.1165/ajrcmb/7.2.190
68. Miakotina OL, Dekowski SA, Snyder JM. Insulin inhibits surfactant protein A and B gene expression in the H441 cell line. *Biochim Biophys Acta*. 1998;1442:60–70. doi:10.1016/s0167-4781(98)00121-3
69. Rayani HH, Gewolb IH, Floros J. Glucose decreases steady state mRNA content of hydrophobic surfactant proteins B and C in fetal rat lung explants. *Exp Lung Res*. 1999;25:69–79. doi:10.1080/019021499270439
70. Zhu Y, Zhang T, Sun D, et al. Profiling maternal plasma microRNA expression in early pregnancy to predict gestational diabetes mellitus. *Int J Gynaecol Obstet*. 2015;130:49–53. doi:10.1016/j.ijgo.2015.01.010
71. Trajkovski M, Hausser J, Soutschek J, et al. MicroRNAs 103 and 107 regulate insulin sensitivity. *Nature*. 2011;474:649–653. doi:10.1038/nature10112
72. Zhang L, Zhang T, Sun D, et al. Diagnostic value of dysregulated microribonucleic acids in the placenta and circulating exosomes in gestational diabetes mellitus. *J Diabetes Investig*. 2021;12:1490–1500. doi:10.1111/jdi.13493